Structure and Dynamics of Blends of Polyhedral Oligomeric Silsesquioxanes and Polyethylene by Atomistic Simulation

Franco M. Capaldi,[†] Gregory C. Rutledge,*[,‡] and Mary C. Boyce[†]

Department of Mechanical Engineering, Massachusetts Institute of Technology, Cambridge, Massachusetts 02139, and Department of Chemical Engineering, Massachusetts Institute of Technology, Cambridge, Massachusetts 02139

Received February 22, 2005; Revised Manuscript Received May 16, 2005

ABSTRACT: The influence of blending polyhedral oligomeric silsesquioxane substituted with cyclopentyl rings (CpPOSS) into a polyethylene (PE) matrix was probed using atomistic simulations. Composites of 5, 15, and 25 wt % CpPOSS were simulated. Interactions between POSS particles were found to promote organization of POSS within the polymer, where clear signs of aggregation were observed. Both particle and polymer dynamics were monitored. Particular attention was given to the structure and dynamics of the interface between particle and polymer. The interface was found to consist of a 3−5 Å thick shell in which the structure of the matrix was altered from that of the bulk. In this region, the local polymer backbone orientation is biased toward a configuration parallel to the particle surface. Dynamically, the interface consists of a thick shell about 11 Å thick in which polymer mobility is damped in the direction normal to and enhanced circumferentially to the surface of the CpPOSS particle. These results suggest that the CpPOSS particles exert an influence on the matrix material which mimics the effects of a rigid surface. A potential of mean force between CpPOSS particles in a polyethylene matrix at 500 K is derived from these atomistic simulation results.

1. Introduction

Polyhedral oligomeric silsesquioxane (POSS) molecules[1,2] consist of an inorganic cage of silicon and oxygen surrounded by organic groups covalently bonded to the silicon atoms. POSS may be incorporated into a polymer either by chemical tethering to the polymer backbone or by blending the particles with the polymer matrix. POSS-tethered monomers have been successfully copolymerized with a wide variety of polymers including polysiloxane,[3−5] poly(methyl methacrylate),[6] polynorbornene,[7] polystyrene,[8] polyethylene,[9] and polyurethane.[10−12] In chemically tethered POSS systems, the incorporation of POSS into various polymers has been linked to increases in glass transition temperature,[13−15] lower viscosities,[16] increased fracture toughness,[17] and improved thermal stability. In blends of PMMA and acrylic polyhedral oligomeric silsesquioxanes, a decrease in the glass transition temperature and melt-state linear visocelastic moduli was observed.[18] The structure of a POSS molecule with cage structure of Si_8O_{12} is shown in Figure 1. The organic groups can be chosen to promote compatibility between POSS and polymer. This paper focuses on blended composites of cyclopentyl-substituted POSS (CpPOSS, $H_{72}C_{40}Si_8O_{12}$) within a polyethylene (PE) matrix.

In polymer matrix composites, the POSS filler has been found to aggregate into small crystalline domains.[11,19] However, the role of these domains in determining the properties of the composite is not clear. At issue is whether a composite morphology with crystalline aggregates or a perfect molecular dispersion of POSS is preferable for achieving different desired properties. For example, experimental Fourier transform infrared spectroscopy (FTIR) studies suggest that it is not the size and rigidity of the POSS particle which cause an increase in T_g for the matrix polymer but that individual isolated particles serve effectively as crosslinks, thereby modifying the polymer dynamics.[13] Previous attempts to model chemically tethered POSS nanoparticles have indicated that well-dispersed POSS particles could increase the glass transition temperature and improve mechanical properties without the presence of aggregates.[20] Simulations of tethered structures at a coarse-grained scale have shown that the linker length and flexibility can greatly affect the properties of the composite in these systems.[21]

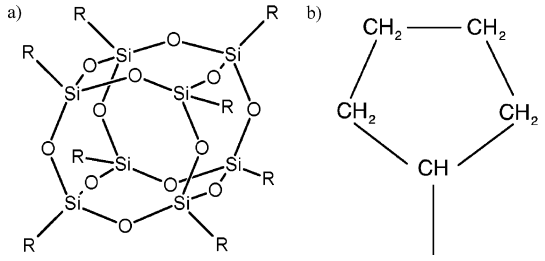

Figure 1. (a) Schematic of the silicate cage ($R_8Si_8O_{12}$). (b) Schematic of the cyclopentyl (C_5H_9) R groups used in this study.

In this paper we simulate blends of POSS in polymer, without tethers. For a given volume fraction, as the size of the filler is decreased and the dispersion is improved, interfacial interactions between filler and matrix become increasingly important in determining the properties of the composite. This paper focuses on the aggregation behavior of the POSS in the polymer and on the interface between nanoparticle and polymer, in an attempt to quantify the effects of POSS on the surrounding polymer matrix.

2. Simulation Details

Three systems were constructed: a 5 wt % CpPOSS/PE composite comprising 6 CpPOSS particles and 158

[†] Department of Mechanical Engineering.
[‡] Department of Chemical Engineering.
* Corresponding author: E-mail rutledge@mit.edu.

10.1021/ma050380e CCC: $30.25
Published on Web 06/29/2005

pentacontane ($C_{50}H_{102}$) chains, a 15 wt % CpPOSS/PE composite comprising 20 CpPOSS particles and 158 pentacontane chains, and a 25 wt % CpPOSS/PE system comprising 60 CpPOSS particles and 167 pentacontane chains. The pentacontane chains were used as models for polyethylene, referred to hereafter as PE for simplicity. The POSS particles and PE were modeled using an explicit atom force field developed by Sun et al.[22−24] The force field was initially developed for use with polysiloxane and alkanes, but lattice dynamics calculations of crystal structure and normal mode vibrational frequencies indicate that this force field captures both the intramolecular bonding and intermolecular packing of CpPOSS.[25] The functional form of this force field is given by

$$E_{\text{total}} = \sum_{b}\sum_{n=2}^{4}[k_n(b-b_0)^n] + \sum_{\theta}\sum_{n=2}^{4}[H_n(\theta-\theta_0)^n] + \sum_{\phi}\sum_{n=1}^{3}[V_n(1-\cos(n\phi))] + \sum_{b,b^*}[k^{bb}(b-b_0)(b^*-b_0{}^*)] + \sum_{b,\theta}[k^{b\theta}(b-b_0)(\theta-\theta_0)] + \sum_{b,\phi}[(b-b_0)\sum_{n=1}^{3}k_n{}^{b\phi}\cos(n\phi)] + \sum_{\theta,\phi}[(\theta-\theta_0)\sum_{n=1}^{3}k_n{}^{\theta\phi}\cos(n\phi)] + \sum_{\theta,\theta^*}k^{\theta\theta}(\theta-\theta_0)(\theta^*-\theta_0^*) + \sum_{\theta,\theta^*,\phi}k^{\theta\theta\phi}(\theta-\theta_0)(\theta^*-\theta_0^*)\cos\phi + \sum_{i,j}\epsilon_{ij}\left[2\left(\frac{\sigma}{r_{ij}}\right)^9 - 3\left(\frac{\sigma}{r_{ij}}\right)^6\right] + \sum_{i,j}\frac{q_iq_j}{r_{ij}} \quad (1)$$

where b is a bond length, θ is a bond angle, ϕ is a torsion angle, r_{ij} is the distance between atoms i and j, and q_i is the charge on atom i which is calculated using bond increments δ_{ij}. This potential accounts for both intermolecular and intramolecular interactions. The force field parameters used within this work are taken from Sun et al.[22−24]

The silicate cage of the POSS particles used in this work is relatively rigid with a cubelike shape having an edge length (Si to Si distance) of 3.16 Å. The length of the cube's edge increases to 7.45 Å when the excluded volume of the constituent atoms is taken into account. The radius of gyration of the PE, unperturbed by the presence of the POSS particles, is estimated to be around 10.9 Å. Monte Carlo calculations for polymer chains that are longer than the filler show increases in the radius of gyration with the addition of the filler.[26] For a particle much larger than the radius of gyration, the polymer might flatten near the surface of the particle as it does near walls.[27,28] In this work, the ratio of chain size to particle size is on the order of one while the ratio of the particle size to the constituent polymer bead is somewhat larger.

Molecular dynamics simulations were performed using the velocity Verlet algorithm[29] with an integration time step of 1 fs. The pressure within the simulation cell was maintained at the target value by rescaling the volume of the cell using the approach of Berendsen et al.[30] with a barostat constant of 100 ps. The temperature was controlled using the Berendsen thermostat with a thermostat constant of 10 ps.

Initial structures were generated by placing POSS particles randomly within the simulation cell. PE chains were introduced into the system by randomly picking a starting point for the chain and inserting additional monomers with fixed bond lengths, fixed bond angles, and random dihedral angles, with an acceptance criteria based on the energy of the inserted molecule. The system was then equilibrated using a Metropolis Monte Carlo algorithm[31] with single atom displacement moves applied to all atoms and reptation moves and concerted rotation moves applied to polymer chains.

Each structure was then subjected to the following simulation schedule: (i) 100 ps simulation at 500 K, holding the number of atoms, volume, and temperature constant (NVT ensemble); (ii) 5 ns simulation at 500 K, holding the number of atoms, pressure, and temperature constant (NPT ensemble); (iii) 2 ns simulation during which the temperature was ramped from 500 to 300 K in steps of 1×10^{-4} K every 1 fs; (iv) 10 ns at 300 K, holding the number of atoms, stress tensor, and temperature constant ($N\sigma T$ ensemble). In each case, the set point pressure was atmospheric. The intent of this protocol was to observe the behavior of the composites at 500 and 300 K, with the cooling segment allowing for an equilibrated structure to be constructed at 300 K. For each system, the entire schedule requires over 500 CPU hours parallelized over eight Pentium III 1.2 GHz machines. The simulation segment (i) allows the atomic velocities to equilibrate before the simulation cell size is allowed to fluctuate. The system densities were 0.82 ± 0.01, 0.84 ± 0.01, and 0.87 ± 0.01 g/cm^3 at 500 K and 0.91 ± 0.01, 0.93 ± 0.01, and 0.96 ± 0.01 g/cm^3 at 300 K for composites of 5, 15, and 25 wt %, respectively.

In addition, simulations of CpPOSS crystals were performed at 300 K in the $N\sigma T$ ensemble using the initial structures based on X-ray crystallography performed by Bassindale et al.[32] These simulations used the same algorithms and time constants as the composite simulations. Results of simulations on POSS crystals using lattice dynamics are presented elsewhere.[25]

3. Results

The incorporation of POSS molecules within the polymer matrix alters the material behavior at different microstructural length scales. First, global structural and dynamical features of the composites are presented, indicating the degree to which particles are attracted to one another and how mobile they are within the composite. Second, more detailed local calculations are presented to reveal the structural changes that occur in the matrix material in the immediate vicinity of the surrounding CpPOSS particles. In addition, changes in the mobility of the surrounding matrix material are also presented. Finally, a potential of mean force between POSS particles embedded in a polymer matrix is derived from the atomistic calculations.

3.1. Characterization of the Composite. 3.1.1 Aggregation. Crystallization of POSS particles has been seen experimentally and can play an important role in determining the properties of the final composite. Significant aggregation increases the effective particle size and thereby also decreases the fraction of interfacial

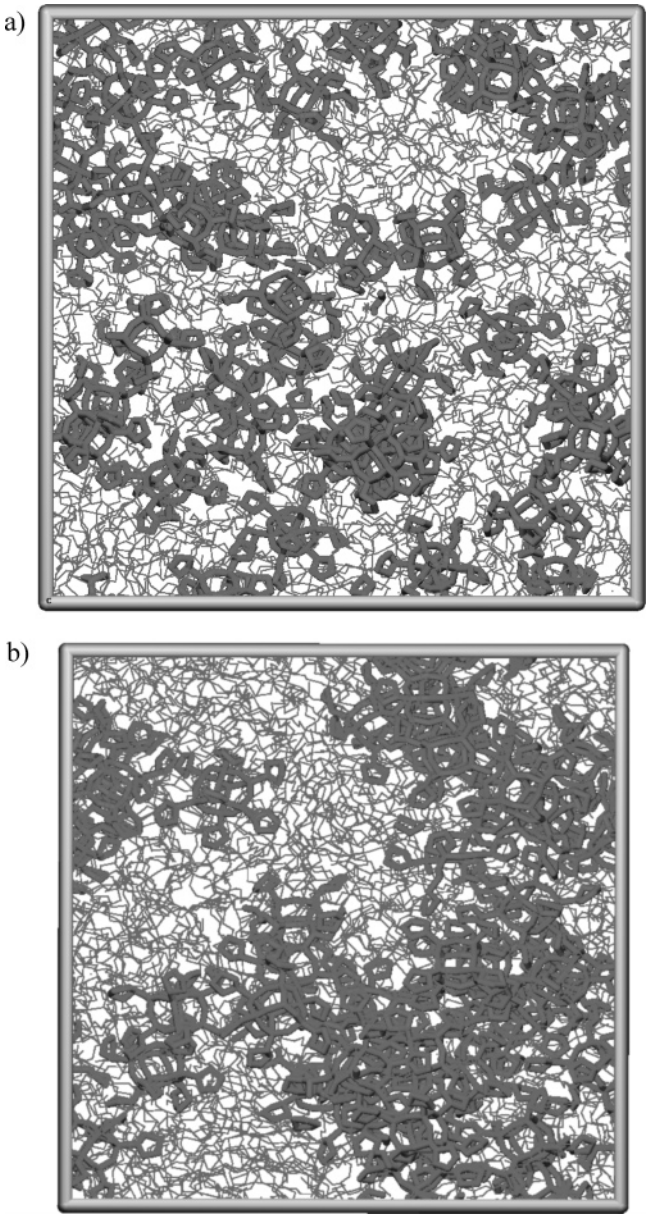

Figure 2. Snapshot of (a) system after equilibration at 500 K for a 25 wt % CpPOSS/PE system with a box length of 66.9 Å and (b) system after cooling to 300 K with a box length of 64.6 Å. CpPOSS particles are dark gray, and PE chains are thin gray lines.

material in the composite. Aggregation also alters the effective properties of the filler inclusion. To study aggregation within these composites, the evolution of structure within the composite was monitored over the time scales accessible within these simulations. Even in simulations as short as 10 ns, changes in structure could be observed that indicate increased ordering of particles. Figure 2 shows snapshots of the 25 wt % system after completing stage ii (500 K) and at the end of stage iv (300 K). POSS particles are initially distributed randomly within the matrix at 500 K. During the 5 ns NPT simulation at 500 K, particle aggregation occurs, but without any internal structure developing. Upon cooling to 300 K, the particles further aggregate within the polymer matrix, with the aggregates now developing an identifiable internal structure.

The aggregate structure was quantified by calculating the radial distribution function between the centers of

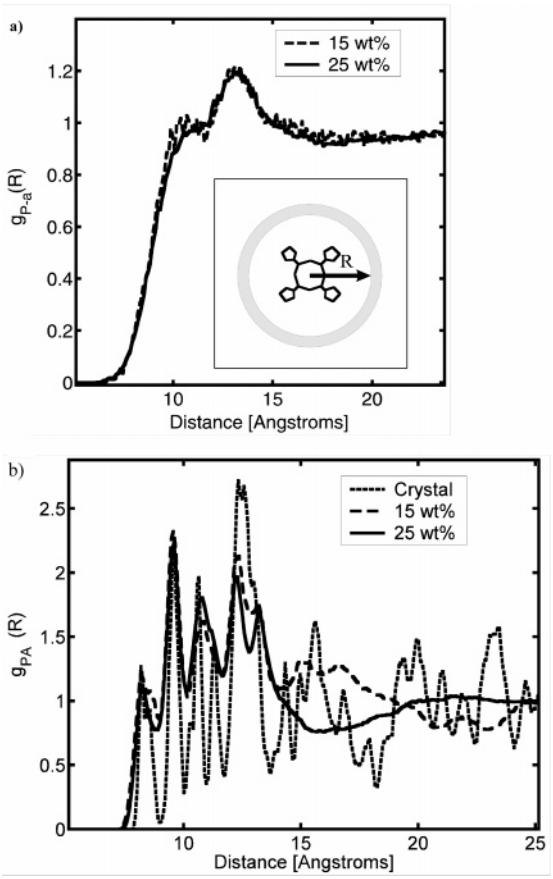

Figure 3. (a) Radial distribution function, $g_{P,A}(R)$, of 15 and 25 wt % CpPOSS/PE composite at 500 K. The inset illustrates the measurement of R from the center of the POSS particle. (b) Radial distribution function, $g_{P,A}(R)$, of CpPOSS crystal, 15% CpPOSS/PE composite, and 25 wt % CpPOSS/PE composite at 300 K.

mass of POSS particles and all silicon atoms within the system belonging to other POSS particles:

$$g_{P,A}(R) = \frac{V}{N_{Si}N_P}\langle\sum_{i=1}^{N_P}\sum_{j=1}^{N_{Si}}\delta(R - |\vec{r}_i^{\,P} - \vec{r}_j^{\,Si}|)\rangle \qquad (2)$$

where $\vec{r}_i^{\,P}$ is the center of mass of POSS particle i, $\vec{r}_j^{\,Si}$ is the position of silicon atom j, V is the volume of the simulation cell, N_{Si} is the number of silicon atoms in the system, and N_P is the number of POSS particles in the system. The only silicon atoms present within the system are located on the cage of the POSS particles. Therefore, this function shows on average how neighboring POSS particles are arranged around any given POSS particle.

Figure 3a displays the radial distribution function at 500 K for the 15 and 25 wt % systems. The structure exhibits only a weak, fluidlike, short-range ordering of silicon atoms at this temperature. This indicates that at 500 K there is no discernible coordination of the CpPOSS particles within the systems. When the system is cooled to 300 K (Figure 3b), the appearance of sharp peaks in the radial distribution function indicates a specific organization of neighboring POSS particles. The peaks are present for distances less than 15 Å (which is the maximum distance between silicon atoms within nearest-neighbor POSS particles). These peaks correspond to the peaks present in the radial distribution function for a CpPOSS crystal, as also shown in Figure

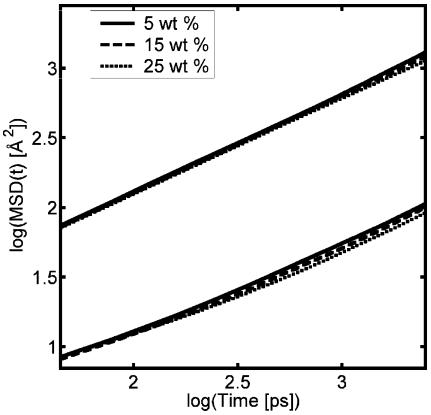

Figure 4. Mean-squared displacement (MSD) of carbon atoms in polymer at 500 and 300 K.

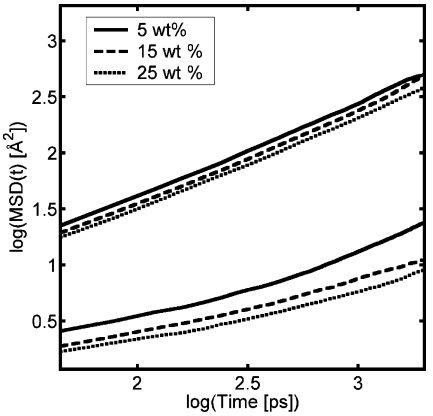

Figure 5. Mean-squared displacement of silicon atoms at 500 and 300 K.

3b. This suggests a clear ordering of neighboring POSS particles into the structural arrangement of the type found in the crystal phase, wherein the organic pendant group of each POSS is aligned with a face of the neighboring silicon−oxygen cage. However, the simulation time scale (10 ns) precludes the formation of well-organized crystals. Instead, multiple POSS particles align with one another in an irregular network. The presence of crystalline domains within POSS/polymer composites has been observed in experiments.[11] The ordered aggregates observed in these simulations are most likely the precursors to the crystallites observed experimentally. Unfortunately, the simulation time scales are too short to observe the assembly of well-formed crystallites. Data from the 5 wt % composite is not shown in Figure 3b because the CpPOSS particles, being more dilute in that system, did not exhibit aggregation on the time scale of the simulation.

3.1.2. Mobility. Understanding the effects of increasing CpPOSS concentration on mobility of both the polymer and the particles is critical to understanding how CpPOSS acts to either reinforce or, alternatively, plasticize the matrix and alter the properties of the composite. These effects were determined by calculating the translational dynamics of the polymer and the translational and rotational dynamics of the CpPOSS particles. The translational dynamics were determined by measuring the mean-squared displacement

$$\langle \Delta r(t)^2 \rangle = \left\langle \frac{1}{N} \sum_{i=1}^{N} (|\vec{r}_i(t) - \vec{r}_i(0)|)^2 \right\rangle \tag{3}$$

of atoms within the system and using these data to calculate a diffusion coefficient, D, for that set of atoms. The diffusion coefficient is obtained from the limiting behavior of the mean-squared displacement using the familiar Einstein relation:

$$\lim_{t \to \infty} \frac{\mathrm{d}\langle \Delta r(t)^2 \rangle}{\mathrm{d}t} = 6D \tag{4}$$

The mean-squared displacement of the carbon atoms along the backbone of the polymer chain is given in Figure 4. The calculated diffusion coefficients in Table 1 reveal that the mobility of the polymer decreases with increasing CpPOSS concentration, at least for the data at 500 K; the data at 300 K are within the margin of error. The slope of the mean-squared displacement in the log−log plot in Figure 4 is ≈0.7, which indicates that the diffusion coefficients most probably are not representative of Fickian diffusion for the polymer chains. However, the calculated range of diffusion coefficients of 5.0×10^{-6}−6.5×10^{-6} cm^2 s^{-1} at 500 K compare well with the experimental value of 6.1×10^{-6} cm^2 s^{-1} extrapolated from data reported by Pearson et al.[33] for $C_{50}H_{102}$ at 500 K.

Table 1. Diffusion Coefficients ($\times 10^6$ D [cm^2 s^{-1}]) for Polymer Backbone Atoms[a]

composition [wt % POSS]	300 K	500 K
0	0.44(3)	6.4(1)
5	0.43(2)	6.5(1)
15	0.44(4)	6.0(1)
25	0.40(8)	5.0(3)

[a] The error in the last significant figure is given in parentheses.

Table 2. Diffusion Coefficients for Silicon Atoms at 500 K and Rotational Relaxation Time for POSS[a]

composition [wt % POSS]	D ($\times 10^6$ [cm^2 s^{-1}])	τ_{rot} [ps]
5	4(1)	403
15	4.0(8)	453
25	3.0(1)	617

[a] The error in the last significant figure is given in parentheses.

To measure the translational mobility of POSS particles, the mean-squared displacement of the silicon atoms within the system was monitored, the results of which are given in Figure 5. The slope of the mean-squared displacement of the silicon atoms in Figure 5 is one, indicating that motion is in the Fickian diffusion regime in this case. The calculated diffusion coefficients in Table 2 reveal that the diffusion of the silicon atoms is ≈1.5 times slower than that of the polymer. Table 2 also displays a drop in mobility at 25 wt % CpPOSS. The diffusion coefficients could not be calculated accurately at 300 K due to the slow motion of the CpPOSS particles at that temperature.

The rotational motion of the CpPOSS particles within the composite was determined by monitoring the reorientation of Si−O bonds within the system. These bonds are found only within the cage of the CpPOSS molecule, and a change in orientation of these bonds is directly related to the rotation of the CpPOSS cage. The autocorrelation function of the bond vector $\vec{b}_i$

$$BACF(t) = \langle b_i(t+\tau)\, b_i(\tau) \rangle \tag{5}$$

was computed for the Si−O bonds and is shown in

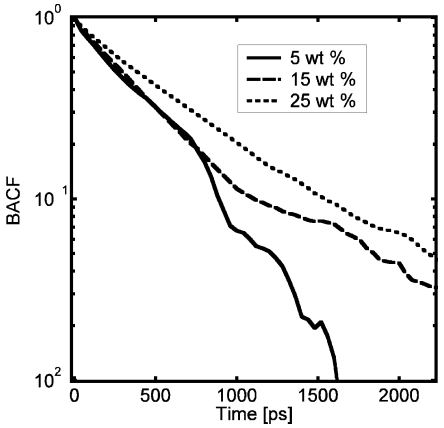

Figure 6. Bond autocorrelation function (BACF) for Si−O bonds at 500 K for 5, 15, and 25 wt % CpPOSS/PE composite.

Figure 6. From exponential fits to the data in Figure 6, the relaxation times for the composites shown in Table 2 were obtained. The rotational relaxation time increases by 50% as the concentration of CpPOSS is increased from 5 wt % to 25 wt %.

The decrease in the mobility of the POSS particles with increasing concentration, in particular as the concentration is increased from 15 wt % to 25 wt %, may be due to the same attractive interactions between particles that leads to the aggregation discussed earlier. At 5 wt %, these attractions appear to be sufficiently minor that the POSS particles may be deemed dilute and noninteracting.

3.2. Characterization of the Interface. Because the silicon−oxygen cages of the POSS molecules are relatively rigid, the interfacial region can be clearly identified with the organic component immediately adjacent to the cage. This includes both matrix polymer and pendant R groups of the POSS molecules. Here we define interfacial material to be the region of matrix material adjacent to the CpPOSS particle where the structure and/or properties differ from those of the bulk matrix material. Significantly, the measured thickness of the interface depends on the particular structural feature or the property used to define the interface. In the following sections, the interface is characterized using both structural (the orientational order parameter) and dynamical (diffusivity) measures.

3.2.1. Orientational Order within the Interface. The alignment and organization of polymeric material near the surface of the CpPOSS particle may have strong effects on the rheology of the melt and on the stiffness of the solid composite. The structure of the polymer was determined by monitoring the orientation of the polymer backbone relative to the radial direction of the CpPOSS particle. The orientation of a segment of the backbone is measured by the vector, $\vec{\nu}_i$, connecting the two carbon atoms bonded to carbon atom i as follows:

$$\vec{\nu}_i = \vec{r}_{i-1} - \vec{r}_{i+1} \tag{6}$$

A vector, $\vec{\rho}_{i,j}$, can then be formed from the center of $\vec{\nu}_i$ to the center of mass of the CpPOSS particle, $\vec{r}_j^{\,P}$, as follows:

$$\vec{\rho}_{i,j} = \left[\frac{\vec{r}_{i-1} + \vec{r}_{i+1}}{2}\right] - \vec{r}_j^{\,P} \tag{7}$$

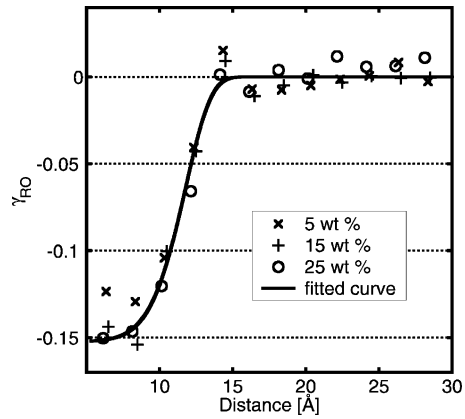

Figure 7. Radial orientation order parameter at 500 K for 5, 15, and 25 wt % CpPOSS/PE composite as a function of distance from the center of a POSS particle. Fitted curve is the negative of a decaying stretched exponential fit to data at all concentrations.

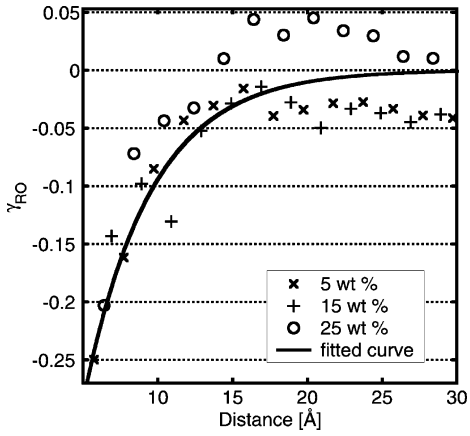

Figure 8. Radial orientation order parameter at 300 K for 5, 15, and 25 wt % CpPOSS/PE composite as a function of distance from the center of a POSS particle. Fitted curve is the negative of a decaying stretched exponential fit to data at all concentrations.

The variation in structure was monitored using the following radial orientation order parameter, which measures the second Legendre coefficient for $\vec{\nu}_i$ as a function of radial distance from the center of a POSS molecule:

$$\gamma_{RO}(R) = \left\langle \frac{1}{N_{CH_2} N_P} \sum_{i=1}^{N_{CH_2}} \sum_{j=1}^{N_P} \frac{3\cos^2(\theta_{i,j}^{\rho\nu}) - 1}{2} \delta(|\rho_{i,j}| - R) \right\rangle \tag{8}$$

where N_{CH_2} is the number of polymer CH_2 groups within the system, and $\theta_{i,j}^{\rho\nu}$ is the angle between the local chain direction, $\vec{\nu}_i$, and the radial vector, $\vec{\rho}_{i,j}$. This function, which is an average over all i and j, takes a value of −0.5 when all vectors $\vec{\nu}_i$ are circumferential to the particle, 1.0 when all $\vec{\nu}_i$ are radially oriented, and 0.0 when the vector pairs $\vec{\nu}_i$ and $\vec{\rho}_{i,j}$ are randomly oriented with respect to one another.

Figures 7 and 8 show the results of applying eq 8 to systems with 5, 15, and 25 wt % CpPOSS/PE composites at 500 and 300 K, respectively. At distances very far from the CpPOSS particle, γ_{RO} is approximately zero, indicating randomly oriented chains, as one would expect for an amorphous material. In all cases, as the

Table 3. Weight Percent of Polymer Found within the Interface[a]

composition [wt % POSS]	300 K	500 K
5	6.8(2)	10.8(6)
15	16.7(3)	27(2)
25	24.4(3)	43(2)

[a] The error in the last significant figure is given in parentheses.

distance R is decreased, the value of $\gamma_{RO}(R)$ also decreases, indicating that the presence of the particle induces circumferential alignment of the polymer chains. The outermost extent of the interface was determined by fitting a stretched exponential to the γ_{RO} data and obtaining the distance, R, at which $\gamma_{RO}(R)$ is equal to 10% of the maximum deviation of γ_{RO} from its far field value. At 500 K structural deviations from bulk matrix orientation can be observed up to 13.3 ± 0.2 Å from the center of mass of the CpPOSS particle. At 300 K the structural differences extend 11.7 ± 0.7 Å from the center of mass of the CpPOSS particle. These calculations also show that the POSS cage excludes polymer out to a distance of ≈5 Å. The quoted range of influence includes both this excluded distance as well as the interfacial width. Given these ranges of influence of the particles on the polymer orientation, the number fraction of monomers located within the interface runs as high as 24% at 300 K and 43% at 500 K for the 25 wt % composite. The values are reported in Table 3.

3.2.2. Polymer Dynamics within the Interface. The structural differences observed in the interface suggest that there might also be differences in the dynamics of the polymer in this region. It has previously been shown that attractive interactions between particle and polymer act to decrease the dynamics of polymer within some region surrounding the particle.[28] If this were true, it would explain the decrease in the overall mobility of the polymer within the composite described earlier.

The atomic mobility was monitored as a function of distance away from the center of the CpPOSS particle. The mean-squared displacement, $MSD(R,\Delta t)$, of polymer carbon atoms which were originally a distance R from the center of the CpPOSS particle after a time Δt has elapsed is given by

$$MSD(R,\Delta t) = \left\langle \frac{1}{N(R,t)} \sum_{j=1}^{N_P} \sum_{i=1}^{N_C} \left| \vec{r}_i(t+\Delta t) - \vec{r}_i(t) \right|^2 \delta(R - |\vec{r}_i(t) - \vec{r}_j^{\,P}(t)|) \right\rangle$$

$$N(R,t) = \sum_{j=1}^{N_P} \sum_{i=1}^{N_C} \delta(R - |\vec{r}_i(t) - \vec{r}_j^{\,P}(t)|) \qquad (9)$$

where $N(R,t)$ is the number of polymer carbon atoms at a distance R from the center of the CpPOSS particle at time t, $\vec{r}_i(t)$ is the position of atom i at time t, $\vec{r}_j^{\,P}(t)$ is the position of the center of mass of CpPOSS particle j, and N_C is the number of polymer carbon atoms in the system. Figures 9 and 10 show $MSD(R,\Delta t)$ calculated at 500 and 300 K, respectively, for a system with 5 wt % POSS. The lack of variation in the mean-squared displacement of atoms as a function of distance from the center of the CpPOSS particle indicates that the overall motion of the polymer backbone is not affected by the presence of the CpPOSS particle. The same behavior is observed in the 15 and 25 wt % CpPOSS composites. It is important to note that when Δt is large, this calculation averages the mobility experienced by a polymer atom as it diffuses and explores regions more or less remote from the CpPOSS particle. As a consequence, we estimate that this function has limited resolving power at 500 K since the polymer backbone is displaced by an average 8.2 Å over 40 ps (12 Å over 120 ps). However, at 300 K the polymer backbone moves an average of only about 2.8 Å over 40 ps (3.7 Å over 120 ps) so the resolution should be adequate.

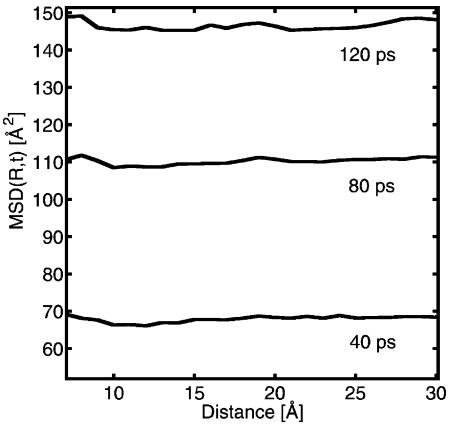

Figure 9. Local mean-squared displacement at 500 K for a 5 wt % CpPOSS/PE composite.

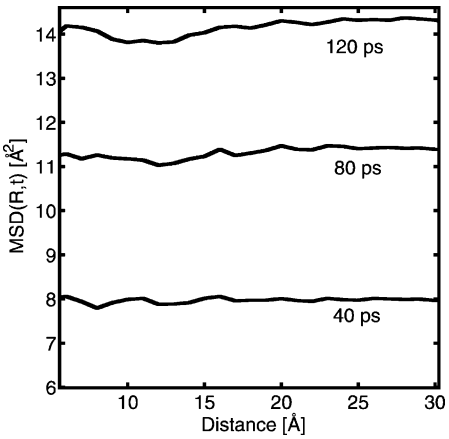

Figure 10. Local mean-squared displacement at 300 K for a 5 wt % CpPOSS/PE composite.

The lack of a change in mobility in the interfacial region indicates a neutral interaction between the CpPOSS particles and the polymer. This also suggests that the change in the overall mobility of the polymer is due to a dampening of mobility throughout the matrix due to the presence of the particles and not simply to localized changes in polymer mobility near the surface of the particle.

3.2.3. Radial and Circumferential Dynamics of Polymer within the Interface. The structural alignment of the backbone does imply however that there should be some anisotropy in the polymer dynamics near the surface of the particle. To monitor this, the mean-squared displacements described above were further resolved into components of motion in the radial, $MSD_r(R,\Delta t)$, and circumferential, $MSD_c(R,\Delta t)$, direc-

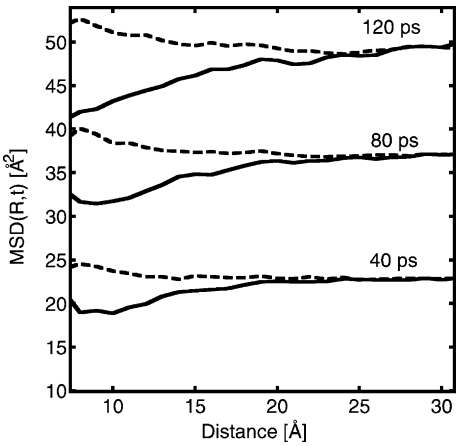

Figure 11. Radial mean-squared displacement as a function of distance from a POSS particle (solid line) and circumferential mean-squared displacement as a function of distance from a POSS particle (dotted line) at 500 K for a 5 wt % CpPOSS/PE composite.

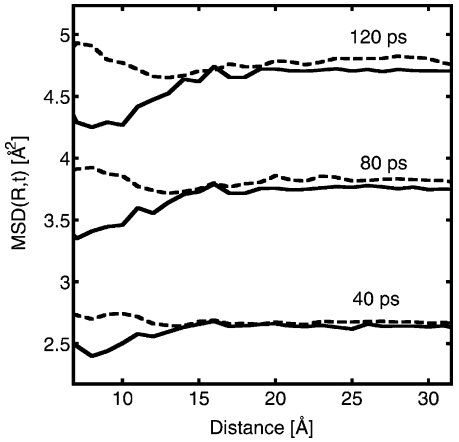

Figure 12. Radial mean-squared displacement as a function of distance from a POSS particle (solid line) and circumferential mean-squared displacement as a function of distance from a POSS particle (dotted line) at 300 K for a 5 wt % CpPOSS/PE composite.

tions, as follows:

$$\vec{\Phi}_{ij} = [\vec{r}_i(t+\Delta t) - \vec{r}_i(t)]\delta(R - |\vec{r}_i(t) - \vec{r}_j^P(t)|)$$

$$MSD_r(R,\Delta t) = \frac{1}{N(R,t)} \sum_{j=1}^{N_P} \sum_{i=1}^{N_C} (\vec{\Phi}_{ij}[\vec{r}_i(t) - \vec{r}_j^P(t)])^2$$

$$MSD_c(R,\Delta t) = \frac{1}{2N(R,t)} \sum_{j=1}^{N_P} \sum_{i=1}^{N_C} (\vec{\Phi}_{ij} - \vec{\Phi}_{ij}[\vec{r}_i(t) - \vec{r}_j^P(t)])^2 \quad (10)$$

Notice that the function representing the mobility in the radial direction measures the mean-squared displacement in a single dimension while the circumferential mobility measures two-dimensional displacement in a plane. To compare the radial and circumferential mobilities, the circumferential mobility is multiplied by a factor of $^1/_2$ in eq 10. This assumes that motion in the plane is isotropic and can be broken down into independent motion along two perpendicular axes within that plane. Far from the CpPOSS particle, MSD_r should be comparable to MSD_c.

Figures 11 and 12 show the component mean-squared displacements for both radial and circumferential motion of the 5 wt % case at 500 and 300 K, respectively. These figures reveal a decrease in mobility in the direction normal to the surface of the CpPOSS and an increase in mobility in the circumferential direction. On the basis of a 10% deviation from its far field value at 80 ps, the radial mobility is decreased out to a distance of approximately 18.4 Å at 500 K and 14.3 Å at 300 K. Similar results were obtained for the 15 and 25 wt % systems. The observed changes in the motion of the polymer near the surface of the particle seem to be due to the structural alignment of the backbone with the particle surface. The interfacial dynamics are modified within a shell of polymer comprising the first two neighbor shells (approximately 11 Å) around the particle. A similar influence out to the second neighbor shell was also suggested by the intermediate scattering function data of Starr et al.,[34] but in that case it must be remembered that the neighbor shells correspond to "monomers" rather than atoms. This would suggest a discrepancy in length scale between the two results, which we believe to be indicative of a breakdown of the coarse-graining approximation for length scales comparable to the size of the coarse-grained bead itself.

3.3. Potential of Mean Force. The importance of aggregation (and possibly crystallization) of these CpPOSS particles within the matrix on determining the properties of the composite is significant. Increases in aggregation lead to decreases in interfacial area and lessen the importance of specific particle/polymer interactions on the structure and dynamics of the polymer within the interface. To understand fully the aggregation and crystallization of CpPOSS particles, it is necessary to conduct simulations on large numbers of CpPOSS particles over long simulated time periods in order to observe the assembly of well-formed crystals. Such simulations are not practical using atomistic level simulations. This practical limitation could be overcome using coarse-grained approximations. In anticipation of this, we derive here an effective interparticle potential of mean force, based on data taken from these atomistic simulations, which can be used for subsequent mesoscopic modeling.

We assume a mesoscopic model which treats CpPOSS particles as interacting spheres. Given a particular functional form, the interaction parameters for the potential of mean force between particles embedded in a polymer matrix at a specific temperature can be found by inverting the observed radial distribution function. The radial distribution function was calculated between the centers of mass of CpPOSS particles, $g_{P,P}$, as follows:

$$g_{P,P}(R) = \frac{V}{{N_P}^2} \langle \sum_{i=1}^{N_P} \sum_{j=1}^{N_P} \delta(R + |\vec{r}_i^P - \vec{r}_j^P|) \rangle \quad (11)$$

Figure 13a shows $g_{P,P}$ for 15 and 25 wt % CpPOSS/PE composites at 500 K. The potential of mean force, $W(r)$, was then calculated by inversion of the Boltzmann distribution:

$$W(R) = -kT \ln(g_{P,P}(R)) \quad (12)$$

where k is Boltzmann's constant and T is the absolute temperature in kelvin. A single potential of mean force was calculated on the basis of the average $g_{P,P}(r)$ for the 15 and 25 wt % CpPOSS composites, as shown in Figure 13b. Strictly speaking, since this potential was derived at 500 K, it is only valid at 500 K. The potential also

Table 4. Potential of Mean Force Model Equations and Parameters

equation	parameters
$W(x) = \begin{cases} ax^5 + bx^4 + cx^3 + dx^2 + ex^1 + f & x \le 13.49 \\ 0 & x > 13.49 \end{cases}$	$a = -0.0168$ kJ/(mol Å^5) $b = 1.1818$ kJ/(mol Å^4) $c = -33.1535$ kJ/(mol Å^3) $d = 462.328$ kJ/(mol Å^2) $e = -320.27$ kJ/(mol Å^1) $f = 8810.1$ kJ/mol
$W(x) = \epsilon\left[2\left(\frac{\sigma}{x}\right)^9 - 3\left(\frac{\sigma}{x}\right)^6\right]$	$\sigma = 1.605$ Å $\epsilon = 11.78$ kJ/mol

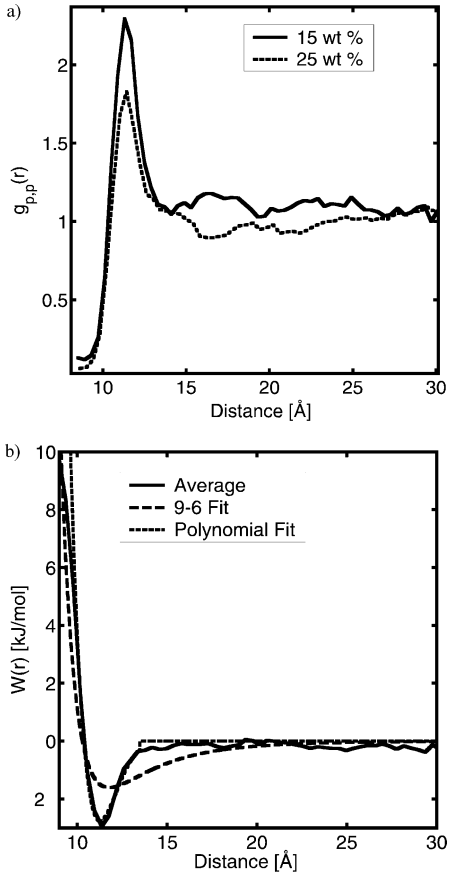

Figure 13. (a) CpPOSS center of mass to CpPOSS center of mass radial distribution function for 15 and 25 wt % CpPOSS/PE composites at 500 K. (b) Potential of mean force for CpPOSS/PE composite at 500 K.

does not capture three-body correlations, which become progressively more important at higher concentrations.

Functions of the Lennard Jones 9−6 type and a fifth-order polynomial were each fit to the data in Figure 13b using a nonlinear least-squares fit. A Lennard-Jones 12−6 type was also tried, but with less satisfactory results. Of these, the polynomial fit was found to yield the best fit. The functions and parameters are given in Table 4.

4. Discussion

In these systems, the CpPOSS particles are initially distributed randomly within the system. During the short time scales of the simulation, irregular aggregates form. Though the simulations cannot be carried out for long enough times to observe directly the formation of large crystals, the relatively quick organization of neighboring CpPOSS particles suggests a strong tendency for crystallization. These simulations clearly illustrate that there exists a thermodynamic driving force favoring the organization of initially well-dispersed

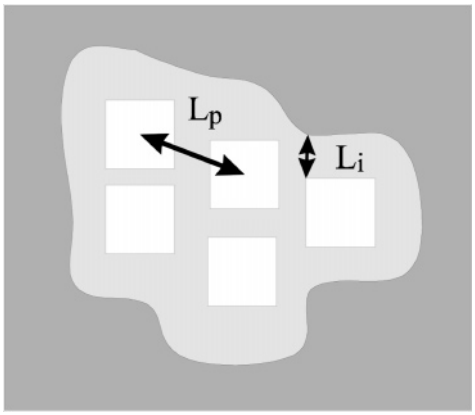

Figure 14. Schematic of small POSS particle aggregate, white squares, within a polymer matrix, dark gray, with an interface of modified polymer surrounding the POSS particles, light gray. The POSS particle center-to-center separation is given by L_p, and the interface thickness is L_i.

CpPOSS particles within this polyethylene matrix. The changes in local orientation of the polymer in the vicinity of the particle are similar to those observed near a wall.[35] The relative importance of these configuration changes clearly depends on the degree of aggregation of CpPOSS particles. Therefore, characterization of this type of composite requires knowledge of not only the POSS particle type and polymer but also the degree of aggregation of particles within the system.

Because of the large surface-to-volume ratio for the nanoscopic CpPOSS particles, there is a significant volume fraction of interfacial matrix polymer within a well-dispersed system. However, this volume fraction becomes less important as the particles aggregate. As shown in Figure 14, the interface extends around the aggregate; with increasing aggregation there is a decrease in the exposed CpPOSS surface area. In the absence of aggregation, and in systems in which the particles do not interact, one would expect the volume fraction of interfacial matrix polymer to increase in direct proportion to the wt % of POSS. Extrapolation of the data from the 5 wt % composite to 25 wt % in this way would imply the number fraction of interfacial matrix polymer should be 54%. Instead, we determined 43% of the monomers were in the interface (Table 3), and the POSS particles were also shown to interact and aggregate. Nevertheless, this reduction in interfacial matrix polymer number fraction is, in our view, modest; we speculate that, had we the liberty to simulate for longer times, this reduction would have been more significant.

These simulations reveal that the polymer within the interface adopts a configuration to accommodate the CpPOSS particle by aligning the polymer backbone tangent to the surface of the CpPOSS particle. While the extent of the interface decreases with decreasing temperature, the degree of alignment within the inter-

face increases. The interactions between the CpPOSS particle and the polymer are governed primarily by the interactions of the cyclopentyl ring groups and the polymer. These interactions are not significantly different from polymer/polymer interactions, and therefore the influence of the particle on polymer dynamics, as measured by a local scalar diffusivity as a function of distance from the particle, appears to be negligible. However, the anisotropy of these dynamics is significantly altered. In the vicinity of the particle, the mean-squared displacement increases in the direction parallel to the surface of the CpPOSS particle, while it decreases in the direction perpendicular to that surface. The anisotropy in dynamics can be attributed to structural alignment near the particle: the polymer can move more easily in the direction of its backbone (i.e., tangential to the particle) through a reptative motion than it can perpendicular to the backbone (i.e., radial to the particle). One might expect the anisotropy in diffusivity observed for the interfacial polymer matrix material to be reflected also in the anisotropic diffusion of small guest molecules. Since the mobility of the polymer is enhanced in the tangential direction, the diffusion of small molecules could also be enhanced in this direction. Therefore, percolation of this aligned layer throughout the entire composite could provide a path for significantly increased diffusion of small molecular species.

The interfacial properties observed within these composite systems are influenced most directly by the geometry of the inclusion and the fact that its movement is slower than that of the polymer. As noted earlier, the CpPOSS particle diffuses at a rate 1.5 times slower than the polymer. We observed a decrease in the diffusion rate of both the polymer and of the CpPOSS, as well as an increase in the rotational relaxation time of CpPOSS, with increasing CpPOSS content. Since there is no decrease in the mobility of the polymer within the interface as compared to the bulk polymer, the decreased dynamics must be attributable to the confinement effect on the polymer from multiple CpPOSS particles. The particles are attracted to one another, and these aggregates not only serve to confine the motion of the polymer but also to hinder the movement of the POSS particles themselves. This is seen in the decreasing POSS particle mobility with increasing concentration.

5. Conclusion

The addition of CpPOSS affects the polymer matrix in several important ways. There is a decrease in the mobility of the polymer within the composite with increasing CpPOSS content due to confinement effects. Aggregates of CpPOSS with clear internal ordering form during the simulations of initially dispersed particles. There exists a layer of polymer surrounding each CpPOSS particle in which the polymer backbone is oriented tangentially to the surface of the particle. In this layer, the polymer exhibits preferential motion tangential to the surface of the particle, which may influence the diffusion of small molecule guest species near the surface of the particle. Although significant fractions of the polymer can be found within the interfacial region in all the simulations performed here, the fraction of polymer located within this interfacial region is dependent on the organization of the CpPOSS particles; aggregation reduces the volume fraction of interfacial matrix polymer. The combined results of each of these effects may help to explain how the properties of the composite as a whole are dependent on the size and amount of CpPOSS aggregation. These results illustrate that phenomena on multiple length scales, from the angstrom length scale interfacial interactions between particles and polymer to the nanometer and micron length scale CpPOSS aggregation, can govern the behavior of these nanocomposite structures.

Acknowledgment. This research was sponsored by the DURINT project monitored by the U.S. AFOSR under Grant F49620-01-1-0447.

Note Added in Proof: A recent manuscript by Striolo, McCabe and Cummings[36] describes molecular simulations of hydrogen- and methyl-functionalized POSS blended with poly(dimethylsiloxane).

References and Notes

(1) Lichtenhan, J. D.; Schwab, J. J.; Reinerth, W. A. *Chem. Innov.* **2001**, *31*, 3−5.
(2) Lichtenhan, J. D. *Comment Inorg. Chem.* **1995**, *17*, 115−130.
(3) Lichtenhan, J. D.; Vu, N. Q.; Carter, J. A.; Gilman, J. W.; Feher, F. J. *Macromolecules* **1993**, *26*, 2141−2142.
(4) Shockey, E. G.; Bolf, A. G.; Jones, P. F.; Schwab, J. J.; Chaffee, K. P.; Haddad, T. S.; Lichtenhan, J. D. *Appl. Organomet. Chem.* **1999**, *13*, 311−327.
(5) Gilman, J. W.; Schlitzer, D. S.; Lichtenhan, J. D. *J. Appl. Polym. Sci.* **1996**, *60*, 591−596.
(6) Lichtenhan, J. D.; Otonari, Y. A.; Carr, M. J. *Macromolecules* **1995**, *28*, 8435−8437.
(7) Mather, P. T.; Jeon, H. G.; Romo-Uribe, A.; Haddad, T. S.; Lichtenhan, J. D. *Macromolecules* **1999**, *32*, 1194−1203.
(8) Zheng, L.; Kasi, R. M.; Farris, R. J.; Coughlin, E. B. *J. Polym. Sci., Polym. Chem.* **2002**, *40*, 885−891.
(9) Zheng, L.; Waddon, A. J.; Farris, R. J.; Coughlin, E. B. *Macromolecules* **2002**, *35*, 2375−2379.
(10) Hsiao, B. S.; White, H.; Rafailovich, M.; Mather, P. T.; Jeon, H. G.; Phillips, S.; Lichtenhan, J.; Schwab, J. *Polym. Int.* **2000**, *49*, 437−440.
(11) Fu, B. X.; Hsiao, B. S.; Pagola, S.; Stephens, P.; White, H.; Rafailovich, M.; Sokolov, J.; Mather, P. T.; Jeon, H. G.; Phillips, S.; Lichtenhan, J.; Schwab, J. *Polymer* **2001**, *42*, 599−611.
(12) Fu, B. X.; Zhang, W. H.; Hsiao, B. S.; Rafailovich, M.; Sokolov, J.; Johansson, G.; Sauer, B. B.; Phillips, S.; Balnski, R. *High Perform. Polym.* **2000**, *12*, 565−571.
(13) Xu, H. Y.; Kuo, S. W.; Lee, J. S.; Chang, F. C. *Polymer* **2002**, *43*, 5117−5124.
(14) Xu, H. Y.; Kuo, S. W.; Lee, J. S.; Chang, F. C. *Macromolecules* **2002**, *35*, 8788−8793.
(15) Choi, J.; Harcup, J.; Yee, A. F.; Zhu, Q.; Laine, R. M. *J. Am. Chem. Soc.* **2001**, *123*, 11420−11430.
(16) Romo-Uribe, A.; Mather, P. T.; Haddad, T. S.; Lichtenhan, J. D. *J. Polym. Sci., Part B: Polym. Phys.* **1998**, *36*, 1857−1872.
(17) Zhang, W.; Fu, B. X.; Seo, Y.; Schrag, E.; Hsiao, B. S.; Mather, P. T.; Yang, N. L.; Xu, D.; Ade, H.; Rafailovich, M.; Sokolov, J. *Macromolecules* **2002**, *35*, 8029−8038.
(18) Kopesky, E. T.; Haddad, T. S.; Cohen, R. E.; McKinley, G. H. *Macromolecules* **2004**, *37*, 8992−9004.
(19) Waddon, A. J.; Zheng, L.; Farris, R. J.; Coughlin, E. B. *Nano Lett.* **2002**, *2*, 1149−1155.
(20) Bharadwaj, R. K.; Berry, R. J.; Farmer, B. L. *Polymer* **2000**, *41*, 7209−7221.
(21) Lamm, M. H.; Chen, T.; Glotzer, S. C. *Nano Lett.* **2003**, *3*, 989−994.
(22) Sun, H. *Macromolecules* **1995**, *28*, 701−712.
(23) Sun, H.; Rigby, D. *Spectrochim. Acta, Part A* **1997**, *53*, 1301−1323.
(24) Sun, H. *J. Phys. Chem. B* **1998**, *102*, 7338−7364.
(25) Capaldi, F. M. Atomistic Simulations of Octacyclopentyl Polyhedral Oligomeric Silsesquioxane/Polyethylene Nanocomposites. Ph.D. Thesis, MIT, 2005.
(26) Yuan, Q. W.; Kloczkowski, A.; Mark, J. E.; Sharaf, M. A. *J. Polym. Sci., Part B: Polym. Phys.* **1996**, *34*, 1647−1657.
(27) Vacatello, M. *Macromol. Theory Simul.* **2004**, *13*, 30−35.

(28) Starr, F. W.; Schroder, T. B.; Glotzer, S. C. *Phys. Rev. E* **2001**, *6402*.
(29) Verlet, L. *Phys. Rev.* **1967**, *159*, 98−103.
(30) Berendsen, H. J.; Postma, J. P. M.; Gunsteren, W. F. v.; Nola, A. D.; Haak, J. R. *J. Chem. Phys.* **1984**, *81*, 3684−3690.
(31) Metropolis, N.; Rosenbluth, A.; Rosenbluth, M.; Tellar, A.; Tellar, M. *J. Chem. Phys.* **1953**, *21*, 1087.
(32) Bassindale, A. R.; Liu, Z. H.; MacKinnon, I. A.; Taylor, P. G.; Yang, Y. X.; Light, M. E.; Horton, P. N.; Hursthouse, M. B. *Dalton Trans.* **2003**, 2945−2949.
(33) Pearson, D. S.; Strate, G. V.; von Meerwall, E.; Schilling, F. C. *Macromolecules* **1987**, *20*, 1133−1141.
(34) Starr, F. W.; Schroder, T. B.; Glotzer, S. C. *Macromolecules* **2002**, *35*, 4481−4492.
(35) Bitsanis, I.; Hadziioannou, G. *J. Chem. Phys.* **1989**, *92*, 3827.
(36) Striolo, A.; McCabe, C.; Cummings, P. T. *J. Phys. Chem. B* (in press).

MA050380E